Loss of class 3 PI3K complex leads to retention of Wg at the apical membrane in polarized tissue

Michaela Holzem[1,2,3,*], Bojana Pavlović[1,2,3], Mareike Munz[1], Jan Gerwin[1], Marko Lampe[4], Fillip Port[1,2,3] and Michael Boutros[1,2,3,*]

[1]German Cancer Research Centre (DKFZ), Division of Signalling and Functional Genomics, Heidelberg, Germany
[2]Institute for Human Genetics, Medical Faculty Heidelberg, Heidelberg University, Heidelberg, Germany
[3]Department of Cell and Molecular Biology & BioQuant, Heidelberg University, Heidelberg, Germany
[4]German Cancer Research Centre (DKFZ), Light Microscopy Core Facility, Heidelberg, Germany
* Corresponding author: m.boutros@dkfz.de and m.holzem@dkfz.de

Keywords: Wnt signaling, Wnt secretion, Wingless, PI3K (III), Vps15, *Drosophila*

ABSTRACT

Wnt signaling plays an essential role in organismal development and stem cell maintenance, and is frequently dysregulated in various human diseases. Wnt proteins are lipid-modified, secreted morphogens that activate biological programs in a concentration-dependent manner. Their secretion depends on specialized trafficking components, including the cargo receptor Evi/Wls, and often involves apical re-internalization and transcytosis. However, several critical steps in Wnt/Wg trafficking remain poorly understood. In this study, we conducted an *in vivo* CRISPR-Cas9 screen in the developing *Drosophila* wing imaginal disc to uncover novel regulators of Wg secretion. We identified Vps15, a regulatory subunit of the class III phosphatidylinositol 3-kinase (PI3K(III)) complex, as an essential factor for Wg trafficking at the apical membrane. Loss of Vps15 leads to pronounced apical accumulation of Wg in producing cells, elevated extracellular Wg levels, and reduced expression of Wg target genes. Our data indicate that PI3K(III) activity is required for efficient apical endocytosis of Wg, independent of Evi/Wls abundance. These findings reveal a previously unrecognized role for the PI3K(III) and lipid biogenesis in Wg secretion within polarized epithelia, enhancing our mechanistic understanding of Wnt trafficking.

Summary statement

We identify the PI3K(III) complex as a novel regulator of Wg endocytosis at the apical membrane, revealing a new mechanism controlling Wnt secretion in polarized epithelial tissue.

INTRODUCTION

The Wnt signaling pathway is one of the key evolutionary innovations at the origin of metazoans (Holstein, 2012; Holzem et al., 2024; Loh et al., 2016). Wnt signaling is essential for patterning the body axes of all multicellular animals and is involved in cell cycle regulation, genome integrity, cell polarity, organismal development and adult homeostasis. Wnt signaling can be divided into three evolutionarily conserved modules: the secretion of Wnt ligands, the trafficking of Wnt molecules to receiving cells, and the reception and activation of intracellular signaling cascades in receiving cells (Alvarez-Rodrigo et al., 2023; Mittermeier and Virshup, 2022). Wnt ligands have been demonstrated to have autocrine, paracrine and endocrine effects (Clevers and Nusse, 2012; Wiese et al., 2018). Upon binding to receptors and co-receptors, Wnt ligands activate different downstream signaling cascades, such as canonical or non-canonical Wnt pathways. Diverse Wnt ligands in combination with various receptors lead to different signaling outcomes, enabling Wnt signaling pathways to activate different physiological programs in a context-dependent manner (Niehrs, 2012; Rim et al., 2022; Wiese et al., 2018).

Wnt/Wg secretion initiates in the endoplasmic reticulum (ER) where Wingless (Wg, human Wnt1) is palmitoylated by the O-acetyltransferase Porcupine (Porcn) and loaded onto the cargo-receptor Evenness interrupted/Wntless (Evi/Wls) (Bänziger et al., 2006; Bartscherer et al., 2006; Goodman et al., 2006). The Evi/Wls-Wg complex is shuttled via COPII vesicles to the Golgi apparatus and further towards the apical plasma membrane. These vesicles fuse with the plasma membrane and expose Wg to the extracellular matrix (ECM). On the apical membrane, Wg protein can traffic via e.g. glypicans such as Dally and Dally-like (Dlp) towards receiving cells (Grobe and Guerrero, 2020; Han et al., 2005; Khare and Baumgartner, 2000; Waghmare et al., 2020; Yan et al., 2009), or can be re-internalized and shuttled via the endosomal pathway into multivesicular bodies (MVBs), which can lead to the apical or basal secretion of Wg on exosomes (Beckett et al., 2013; Gross, 2021; Gross, 2021). Secretion on cellular protrusions, such as filopodia, was also observed on the basal membrane in *Drosophila* (Routledge and Scholpp, 2019; Sharma and Chaudhary, 2024; Stanganello et al., 2015; Wolf and Boutros, 2023). Upon binding of Wg to Frizzled (Fz) receptors and LRP5/6 co-receptors (Arrow in *Drosophila*) on the

receiving cell, intracellular Dishevelled (Dsh) proteins are recruited to the activated receptor complex, activating the assembly of the so-called signalosome (consisting of CK1a, APC, Shaggy (Sgg), Axin and Dsh), which prevents the degradation of Armadillo (Arm, beta-catenin in vertebrates). Arm can subsequently translocate into the nucleus and activate transcription of target genes such as *distalless, senseless, vestigial* or *naked* and others in a concentration and cell-type dependent manner (Alvarez-Rodrigo et al., 2023; Mittermeier and Virshup, 2022; Swarup and Verheyen, 2012; Widmann and Dahmann, 2009).

Since the discovery of the pathway in the 1980s, many components and mechanisms have been discovered and described (Baker, 2024; Jenny and Basler, 2014) and a complex picture of Wnt secretion and signalling has emerged. Genetic screens have identified important components of the Wnt signalling pathway in *Drosophila* (Chaudhary and Boutros, 2019; Evron et al., 2021; Gross et al., 2012; Kramps et al., 2002; Nüsslein-Volhard et al., 1984; Swarup et al., 2015). In the 1980s and 90s, genetic screens primarily used chemical mutagenesis and uncovered many core components of Wnt signalling. However, achieving saturation in such forward genetic screens is challenging. More recently, reverse genetic screens based on RNAi systematically targeted specific subsets of genes, such as kinases, phosphatases or transcription factors, resulting in the identification of additional Wnt pathway components. However, these approaches are limited to genes for which the partial knockdown typically induced by RNAi is sufficient to produce detectable phenotypes. As a result, our current understanding of Wnt signaling remains incomplete. For example, the precise mechanism of Wg secretion from polarized tissues, including its loading onto Dally or Dlp and the mechanism of endocytosis remain incompletely characterized. Further, the spatial and temporal separation between Wg and the cargo-receptor Evi/Wls remains unknown.

Here, we identify novel components involved in Wnt secretion in the polarized cells of the *Drosophila* wing imaginal disc by CRISPR mutagenesis screening. We performed a kinome and phosphatome-wide Cas9-mediated mutagenesis screen to identify proteins which influence the secretion of Wg from the epithelium. Our screen identified Vps15 as a gene required for correct protein trafficking of Wg. Loss of Vps15 results in a strong increase of Wg protein in the apical domain of Wg expressing cells in the wing disc. Vps15

(previously known as *ird1* in *Drosophila* and PIK3R4 in humans) is the regulatory subunit of the class III phosphatidylinositol 3-kinase (PI3K (III)), also known as Vps34 complex (Panaretou et al., 1997; Shravage et al., 2013; Wu et al., 2007). We show that mutagenesis of Vps15 results in a reduction of Wnt target gene expression and impairs Wg endocytosis at the apical membrane of ligand producing cells. The cargo-receptor Evi/Wls does not phenocopy the strong Wg accumulation, suggesting that the accumulation of Wg occurs after the separation of these two proteins. We propose that phospholipids produced by PI3K (III) are important for the re-endocytosis of Wg at the apical plasma membrane and its shuttling towards the early endosome for further distribution and secretion.

RESULTS

A CRISPR-Cas9 screen to identify novel genes for Wnt secretion in *Drosophila*

To identify novel genes involved in Wg secretion, we performed an *in vivo* genetic screen in *Drosophila* imaginal wing discs using tissue-specific CRISPR-Cas9 mutagenesis (Port et al., 2020). We combined an optimized Cas9 transgene with sgRNAs of the HD_CFD library, a large-scale collection of sgRNA transgenes, each expressing two sgRNAs targeting two independent positions per gene (Port et al., 2014; Port et al., 2020). Cas9 expression was induced by the *hedgehog-Gal4 (hhGal4)* driver specifically in the posterior half of the wing disc, which allows for the comparison of perturbed and unperturbed cells side-by-side in the same tissue (Fig. 1A). Acute CRISPR mutagenesis in somatic tissues leads to the generation of small insertions and deletions (indels) at the target locus, which frequently induces loss-of-function alleles. However, the heterogeneous nature of the induced mutations and limitations to CRISPR activity typically result in genetic mosaics, where cells with and without gene disruption are present in the same tissue (Port and Boutros, 2022). To visualize Wg protein we utilized a previously described insertion of GFP in the endogenous *wg* locus (Wg::GFP) (Port et al., 2014). In addition, we used a transcriptional reporter of the Wnt target gene *distalless* (*dll*, Dll::dTom*)* (Chaudhary et al., 2019) (Fig. 1A). In control animals which expressed sgRNAs targeting a gene not expressed in wing imaginal discs, Wg::GFP and Dll::dTom were present at similar levels in the anterior and posterior compartment of the wing disc

(Fig. 1B-B''). In contrast, cells which expressed Cas9 and *Evi/Wls-sgRNAs* had strongly elevated levels of Wg::GFP in Wnt producing cells, a consequence of a block in protein secretion (Bänziger et al., 2006; Bartscherer et al., 2006), and showed reduced expression of the Wnt target gene *dll* (Fig. 1C-C'').

We performed a targeted screen focused on genes encoding kinases or phosphatases, proteins known to be central regulators of intracellular signaling. The HD_CFD library contains sgRNA lines targeting 288 of the 327 kinases encoded in the *Drosophila* genome, and 115 of the 186 phosphatases (Suppl. Table S1). These include 51 genes which have been implicated in Wg regulation in previous screens, which can be used to estimate the efficiency of the screen (Chaudhary and Boutros, 2019; Gross et al., 2012; Swarup et al., 2015) (Suppl. Table S2).

In total, we screened 605 sgRNA lines targeting 411 unique genes and uncovered 56 genes that reduce or increase Wg in the wing disc. Of these, 50 genes have been described to control Wg in previous RNAi based screens, representing a 98% overlap, suggesting high efficiency of our CRISPR perturbations. In addition, we identified Wg phenotypes with 6 lines targeting genes so far not implicated in Wg trafficking, which showed an increase or decrease of Wg signal at the DV boundary. The induction of DNA double-strand breaks through CRISPR nucleases is known to result in frequent mitotic recombination (Allen et al., 2021; Brunner et al., 2019) which can result in loss of heterozygosity of the Wg::GFP or Dll:dTom reporters if induced between their locus and the centromere. We therefore rescreened any genes located between the centromere and the *wg::GFP* gene on chromosome arm 2L by *anti-wg* immunohistochemistry. This revealed that the phenotypes for two of the initial hits reflect mitotic recombination rather than regulation of Wg. The remaining four positive hits showed reproducible effects on Wg protein (Suppl. Table S3).

For further characterization, we selected Vps15, which after CRISPR mutagenesis resulted in the strongest increase in Wg at the DV boundary and which has so far not been implicated in the regulation of Wnt protein secretion. Vps15 forms together with Atg6 and Vps34 the class 3 PI3K complex (Panaretou et al., 1997; Shravage et al., 2013; Wu et al., 2007). PI3K (III) is responsible for the phosphorylation of phosphatidylinositol (PtdIns or PI) to phosphatidylinositol-3-phosphate (PtdIns3P or PI3P). PI3Ps are

membrane associated and are bound by proteins containing FYVE or PX domains (Chandra et al., 2019; Hayakawa et al., 2004; Hurley, 2006; Lemmon, 2003; Shravage et al., 2013; Stenmark et al., 1996; Wurmser et al., 1999), thereby recruiting proteins to specific membrane domains and regulating intracellular trafficking (Abe et al., 2009; Hurley, 2006; Mills et al., 1998; Simonsen et al., 1998; Stenmark et al., 1996; Wurmser et al., 1999). The PI3K (III) complex is known to be involved in the endosomal pathway, formation of MVBs, autophagy and regulate intracellular signal transduction (Abe et al., 2009; Backer, 2008; Rusten et al., 2004; Shravage et al., 2013).

Wg protein accumulates at the apical surface in Vps15 mutant wing imaginal discs

Strong Wg accumulation was observed at the DV boundary and in other *wg* expression domains in Vps15 perturbed posterior wing disc tissue (*Vps15-sgRNA#009*) (Fig. 2A,A'). To validate this phenotype, we used a second sgRNA line from a different sgRNA library (*Vps15-sgRNA#83822*, BDSC) which mediated the same phenotype (Fig. 2C,C'). In both cases Wg accumulated not uniformly across the P-compartment, likely reflecting genetic mosaics induced by the acute CRISPR mutagenesis. To exclude that the accumulation of Wg at the DV boundary is due to increased gene expression, we performed fluorescent *in situ* hybridisation (FISH) of *wg* transcripts. No increase of *wg* mRNA was detected suggesting that the increased Wg abundance arises through misregulation of Wg protein trafficking or turnover (Suppl. Fig. S1A-B). We further analysed the localization of Wg within Vps15 perturbed cells and found that Wg protein mainly accumulates in large puncta at or close to the apical membrane (Fig. 2B,B' and D,D').

We also performed RNA interference (RNAi) experiments using the same *hh-Gal4* driver line as in the CRISPR-Cas9 screen. Three publicly available RNAi lines were tested and none resulted in a similar Wg phenotype than the two sgRNA lines (Suppl. Fig. S1C-E). This suggests that knockdown of Vps15 does not lead to a sufficient reduction of Vps15 expression to affect Wg trafficking, providing a likely explanation why this gene has not been detected in previous RNAi screens.

Perturbations of Wnt signalling and loss-of Wg function are known to affect morphogenesis of the adult wing. These phenotypes can range from a reduction of wing margin bristles, to notches of the margin and up to the complete loss of adult wings. Wings

can therefore be used as a phenotypic readout for malfunctioning Wnt signalling. Mutagenesis of Vps15 is lethal during late larvae/pupal stages when induced by the *hh-Gal4* driver, precluding analysis of adult wings. We therefore induced CRISPR mutagenesis with a different Gal4 driver, with an expression pattern that is much more restricted to the developing wing (*w-;;pdm2-Gal4,UASCas9uM/Tm6B*). Crosses with the *Vps15-sgRNA#009* or *Vps15-sgRNA#83822* lines resulted in viable flies with malformed wings. We observed for *Vps15-sgRNA#009* a vein phenotype in 62.2% of females (n=23) and 46.2% of the male offspring (n=12). In male wings specifically, we also detected bubbles (15,4%; n=4), where the attachment between the dorsal and ventral layer of the wing is disrupted, as well as some notches (3.8%; n=1) (Fig. 2F,H). No disturbed bristles patterns were observed in these samples. 35.1% (n=13) of female and 23.1% (n=6) of male wings did not show a phenotype and resemble wildtype wings (Fig. 2E). We also analysed the wings from the *Vps15-sgRNA#83822* line crossed to the *w-;;pdm2-Gal4,UASCas9uM/Tm6B* driver line. Here, 100% (n=32 for both sexes) of all female and male wings showed a phenotype. All wings were malformed and showed a vein phenotype. Additionally, 15.6% (n=5) of female and 28.1% (n=9) of male wings showed notches at the wing margins, including a loss of bristles in the corresponding area (Fig. 2G). A disturbed bristle pattern was detected in 28.1% (n=9) of female and 31.3% (n=10) of male wing samples, without forming a notch (Fig. 2H). Overall, perturbation of *Vps15* with either sgRNA line resulted in wing abnormalities of which some are consistent with a disruption of Wnt signaling. Others, such as a deregulation of wing vein formation, suggest that Vps15 perturbation might also affect other signalling pathways in the wing epithelium.

Mutagenesis of Vps34 or Atg6 phenocopies the Vps15 phenotype in wing imaginal discs

Vps15 encodes the regulatory subunit of the PI3K (III) complex, which includes two other main components: Atg6 (Beclin-1 in humans or VPS30 in yeast) and Vps34 (human Pik3c3) (Funderburk et al., 2010; Herman et al., 1991; Kihara et al., 2001; Linassier et al., 1997; Panaretou et al., 1997; Shravage et al., 2013). We therefore tested if disruption of the other PI3K (III) components also disrupts Wg homeostasis. We used publicly

available sgRNA lines for disruption of either gene and analysed the effects on Wg::GFP (*Atg6-sgRNA#80830*, BDSC and *Vps34-sgRNA#92484*, BDSC). We found that mutagenesis of Atg6 also led to an accumulation of Wg in the wing disc, in line with previous results (Fig. 3A,A') (Abe et al., 2009; Lőrincz et al., 2014). Similar to cells mutant for Vps15, Wg accumulated predominantly in the apical domain of the cells (Fig. 3B,B'). Furthermore, also loss of Vps34 resulted in an increase in Wg protein at the DV boundary (Fig. 3C,C'), with wg protein being concentrated in puncta at the apical membrane (Fig. 3D,D'). From these results, we conclude that the mutagenesis of Atg6 and Vps34 phenocopies the Wg accumulation resulting from perturbation of Vps15. Hence, all components of the PI3K (III) complex show a similar Wg accumulation at the apical membrane in wing imaginal discs, suggesting this phenotype arises due to loss of PI3K (III) activity.

Vps15 mutagenesis reduces downstream Wnt target gene expression

We next investigated the effects of Vps15 mutagenesis on downstream Wnt signalling such as the low-threshold target gene Dll (Fig. 3A-A'') and the high-threshold gene *senseless* (*sens*) (Fig.3B-B''). We used Dll::dTom to identify effects of Vps15 perturbation on this Wnt target gene. CRISPR mutagenesis with either *Vps15-sgRNA#009* or *Vps15-sgRNA#83822* resulted in a reduction of Dll transcription in the posterior compartment (Fig. 4A-A'', shown for *Vps15-sgRNA#83822,* n=5). We measured the fluorescence intensity of Wg::GFP and Dll::dTom, covering anterior and posterior tissue in an equal proportion at the DV boundary and plotted the average fluorescence intensities. This revealed the strong increase of Wg::GFP in the posterior half and a reduction of Dll::dTom (Fig. 3D). In contrast, the fluorescence signal of Wg::GFP and Dll::dTom in a control cross with *sepia-sgRNA* (n=3) is comparable in both halves of the epithelium (Fig. 3C). These results suggest that loss of Vps15 inhibits downstream Wnt signalling.

To confirm this effect on Wnt signaling, we additionally performed immunohistochemistry for Sens, a second Wg target gene, using the *Vps15-sgRNA#009* line. Since the intensity of Sens expression differs naturally between the anterior and posterior compartments of the wing disc and evolves during development, we examined wing discs with Vps15 clones flanked by wildtype tissue. A reduction of Sens expression

could be detected in the Vps15 mutated area, marked by the strong Wg::GFP accumulation (n=6) (Fig. 4B-B’’).

From these results we conclude that Vps15 mutagenesis impacts downstream Wnt target gene expression. We also conducted the analysis of Wnt target gene expression in Atg6 and Vps34 perturbed tissue. This confirmed that both PI3K (III) subunits phenocopy the effects of Vps15 perturbation, as we observed a reduction in *Dll* and *sens* expression (Suppl. Fig. S2). Taken together, this data indicates that the loss of either subunit of the PI3K (III) complex leads to a reduction of Wnt target gene expression. This suggests that in Vps15 perturbed tissue the secretion of Wg or its trafficking towards receiving cells is negatively affected. Alternatively, loss of PI3K (III) activity could impact signal transduction or gene expression cell autonomously.

Vps 15 perturbation has no effect on Evi/Wls abundance

Evi/Wls binds Wg and shuttles it through the cell towards the plasma membrane. In wing imaginal discs Evi/Wls protein accumulates in Wg positive structures in the apical domain of Wnt expressing cells (Port et al., 2008). We therefore tested if Evi/Wls- loaded vesicles also accumulate in Vps15 perturbed cells. To test this, we used immunohistochemistry with a specific *anti-Evi/Wls* antibody in Vps15 perturbed tissue together with the endogenously labelled Wg::GFP and Dll::dTom. Surprisingly, we did not observe an increased accumulation of Evi/Wls in Vps15 mutated tissue (Fig. 5A-A’’). Evi/Wls protein levels were comparable in both anterior and posterior disc compartments or slightly reduced in the posterior compartment, whereas strong accumulation of Wg was observed in the same tissue (Fig. 5B-B’’).

We also measured the fluorescence intensity of Wg and Evi/Wls (n=6), normalised the data and plotted them into the same graph confirming that Evi/Wls expression is not affected upon Vps15 mutagenesis (Fig. 5C). Based on these results, we hypothesise that Wg trafficking is affected after the separation of the Evi/Wls-Wg complex or the Vps15 perturbation is driving the separation of this complex.

Vps15 mutagenesis leads to an accumulation of extracellular Wg at the apical membrane

Next, we investigated where Wg accumulates in Vps15 perturbed cells. We performed immunohistochemistry to visualize various markers of cellular compartments, such as the endoplasmatic reticulum (anti-*Cnx99a*), the Golgi-apparatus (anti-*Golgin84*), the plasma membrane (anti-*Dlg1*), early (*anti-Rab5*) and late endosomes (*anti-Rab7*) as well as autophagosomes (*anti-Atg8*). The prominent accumulations of Wg::GFP observed in Vps15 mutant cells mainly localized in the same plane as Dlg1, indicating they are located in or adjacent to the apical plasma membrane (Suppl. Fig.S3).

Since PI3K (III) is known to regulate endocytosis through the generation of Pi3P, we analysed whether Wg is retained at the apical membrane. We performed an altered immunohistochemistry protocol without any permeabilization step. With this strategy, it is possible to selectively label extracellular Wg protein, while no labelling occurs intracellularly (Strigini and Cohen, 1999). Additionally, the GFP tag of Wg::GFP also allowed us to detect total Wg protein in the same tissue. Interestingly, we observed an increase of extracellular Wg (Wg^{Ex}) in the Vps15 perturbed areas (Fig. 6A-A''). Wg^{Ex} accumulates to lower levels than total Wg protein and is located slightly apical of the bulk of the Wg::GFP (Fig. 6B-B'', C (n=3)). This suggests that in Vps15 mutant cells Wg reaches the plasma membrane and protein accumulation is likely caused by a defect in onward trafficking, for example endocytosis to lateral spreading to neighboring cells.

We analyzed whether Vps15 perturbation affects the formation of the Wg protein gradient. To assess this, we measured and plotted the spread of Wg^{Ex} fluorescence intensities in both perturbed and unperturbed regions of the same imaginal disc (Fig. 6D). The distribution of fluorescence measurements reflects the range of the gradient within the tissue. Although the intensity curves from perturbed and unperturbed tissues differ in amplitude - indicating a stronger signal in the perturbed region (see above) - they exhibit a similar overall shape (Fig. 6E, n=16). To further characterize potential differences in gradient formation, we examined the slope of each curve and their intersections with the x-axis (Fig. 6F). Derivative analysis revealed that both curves intersect the x-axis at similar positions (Fig. 6F, black arrows), suggesting comparable rates of gradient range. Overall, this analysis indicates no significant difference in the spatial distribution of the

Wg gradient between perturbed and unperturbed tissues. These findings suggest that Wg protein can still be exported and trafficked from producing cells in the absence of PI3K (III) activity.

PI3K (III) complex regulates endocytosis of apical Wg

We analysed whether Wg protein accumulates at the apical membrane due to a malfunction in endocytosis. To address this question, we performed a "Wg uptake assay" that specifically labels Wg protein exposed to the extracellular environment and subsequently internalized (Witte et al., 2021). In this assay endocytosed Wg can be detected intracellularly (Wg^{In}), while none or a reduced amount of Wg protein is detectable inside the cell if endocytosis is impaired (Fig. 7A). We performed the Wg uptake assay in wing imaginal discs expressing Wg::GFP, which allowed us to visualize total and endocytosed Wg in the same tissue (w-;*Wg::GFP,Dll::dTom; hhGal4UASuMCas9/Tm6b*).

In wildtype cells Wg was efficiently endocytosed and Wg^{In} localized to puncta below the apical membrane of the epithelium, likely representing endosomal compartments. In contrast, in Vps15 mutant cells Wg^{In} was found mainly in one apical plain, possibly the plasma membrane (Fig. 7B''). We measured the average fluorescence intensity in three different areas (apical, middle and basal; n=10) (Fig. 7C) and found that while in the apical area the fluorescence signal for Wg^{In} was increased (Fig. 7D), in the middle area of the perturbed tissue there was a slight reduction of the respective signal (Fig. 7E). No differences in Wg levels were detected in the basal area of the epithelium (Fig. 7F). These data suggest that in the absence of Vps15 Wg is not efficiently endocytosed and accumulates at and below the apical membrane.

This is further supported by STED super resolution microscopy of Wg^{In} in cells with and without mutations in Vps15 (Fig. 7G-G'). With the higher resolution we were able to detect small Wg dots in the cytoplasm of unperturbed tissue (white arrowheads) as well as larger accumulations of Wg (white arrows; Fig. 7G'). Only few small Wg puncta were observed in the Vps15 perturbed half of the tissue (Fig. 7G'). We were also able to detect that the Wg^{In} and Wg::GFP labelled pools overlapped both at the apical membrane and intracellularly (Fig. 7 B'-B'''). Taken together, these results suggest that Wg endocytosis

is disturbed upon Vps15 perturbation, likely resulting in the apical accumulation of Wg in producing cells.

DISCUSSION

In this study, we identified novel components involved in *Drosophila* Wg secretion through a kinome and phosphatome-wide CRISPR-Cas9 screen combined with visualisation of endogenously tagged Wg protein. Our screen revealed *vps15* as a critical gene required for Wg protein trafficking in *Drosophila* wing imaginal discs. Upon *vps15* perturbation, we observed a striking accumulation of Wg protein at the apical membrane. Disruption of Vps15 also impacted downstream Wnt signaling, as evidenced by reduced target gene expression (Dll and Sens) and adult wing phenotypes. Our investigations determined that Wg protein accumulated specifically at or near the apical plasma membrane, where it remains capable of forming a protein gradient. Furthermore, we demonstrated that Vps15 perturbation resulted in impaired endocytosis of Wg protein. Based on these findings, we propose that PI3K (III) plays an essential role in the endocytosis of Wg at the apical plasma membrane and its subsequent shuttling toward the endosomal pathway for further basal Wg secretion or transcytosis.

In vivo CRISPR in combination with endogenously tagged readout genes proved to be a powerful tool for screening in *Drosophila*. We readily identified candidates like *myopic (mop), microtubule star (mts), Protein phosphatase 1α at 96A (Pp1alpha-96A), myotubularin (Mtm) or Casein kinase Iα (Ck1alpha)*, which have been previously described as Wnt regulators (Swarup et al., 2015). Overall, the majority of the previously identified genes involved in Wnt signalling or secretion and present in our sgRNA library were also identified in our screen, demonstrating good concordance of CRISPR mutagenesis with previous technologies. In addition, our screen also identified a small number of novel genes. The Wnt pathway regulator we describe here, Vps15, was included in some of the previous RNAi screens, but not identified as a regulator of Wg secretion (Chaudhary and Boutros, 2019; Gross et al., 2012; Port et al., 2011; Swarup et al., 2015). We confirmed here that this is likely due to the very mild or absent Wg phenotype following knock-down of Vps15 using publicly available RNAi lines. In contrast, CRISPR mutagenesis results in strong effects on Wg protein, demonstrating the potential

of CRISPR screens to identify genes that only cause phenotypes upon complete removal of the encoded protein.

Loss of Vps15 function leads to a strong apical Wg accumulation in epithelial cells. This accumulation is phenocopied by perturbation of Atg6 or Vps34, the other two subunits of the PI3K (III) complex, demonstrating that the Wg phenotype is a specific consequence of loss of PI3K (III) function and that all subunits are required. It was previously shown that knockdown of Atg6 leads to the accumulation of Wg at the DV boundary in wing imaginal discs (Abe et al., 2009; Lőrincz et al., 2014), but these studies did not investigate the cellular and mechanistic cause of this phenotype. Our study addresses these questions and shows that a defect in Wg endocytosis in ligand producing cells is the underlying reason for protein mis-localisation. This is consistent with the known function of PI3K (III) of producing PI3P, which is specifically enriched in membranes of endocytic or endosomal vesicles and required for their formation and maturation (Backer, 2000; Balla, 2013; Lindmo and Stenmark, 2006; Tuma et al., 2001). Interestingly, the Wg protein gradient appears to form normally in Vps15 mutant tissue, despite a reduction in the expression of Wnt target genes. It has been described that Wg can be shuttled and secreted via several routes in the wing disc epithelium. The “direct” secretion on the apical membrane involves shuttling of Wg to glypicans such as Dally and Dlp which harbor long lipid chains. These lipid chains form an adaptor surface for Wg protein and can transport Wg towards a receiving cell (Grobe and Guerrero, 2020; Khare and Baumgartner, 2000; Waghmare et al., 2020; Yan et al., 2009). In addition, Wg can also be endocytosed from the apical membrane and directed into the endosomal pathway (Brunt and Scholpp, 2018; Hemalatha et al., 2016), from where it can be loaded on exosomes or trafficked towards the basal membrane or filopodia (Brunt and Scholpp, 2018; Gross, 2021; Gross et al., 2012; Moti et al., 2019; Stanganello and Scholpp, 2016). Loss of the PI3K (III) function appears to only impact “indirect” Wg secretion via endocytosis and might be a valuable tool to further dissect the relative importance of the different secretion routes in the future.

No accumulation of the Wg cargo-receptor Evi/Wls was observed in Vps15 perturbed tissue. This suggests that separation of Wg from its cargo receptor occurs before reinternalization from the plasma membrane. Alternatively, the reduced levels of

PI3P could cause premature separation of Evi/Wls from Wg. In any case, trafficking of Evi/Wls protein, which is known to cycle between the ER and plasma membrane and pass through endosomal compartments, is much less sensitive to a loss of PI3K (III) function than its cargo protein. Previously, it has been suggested that differences in pH of different endomembrane carriers is a driving force for the separation of Evi/Wls from Wg (Coombs et al., 2010; Sharma and Chaudhary, 2024). Still, our data suggests that an apical and pH independent mechanisms might also exist in ploarized tissues. In the future blockage of Wg trafficking at different stages along the secretion and endosomal maturation pathway should shed light on the exact stage of separation of the two proteins.

Overall, our results show that PI3K (III) is required for endocytosis of Wg at the apical membrane, while not affecting protein spreading in adjacent cells. This work adds to our understanding of the molecular regulation of Wnt secretion and distribution in polarized epithelia.

METHODS AND MATERIALS

Fly husbandry and fly lines

All fly lines were kept at 25°C with a 12/12-hour light/dark cycle. Temperature sensitive stocks were kept at 18°C and transferred to 25°C, 29°C or 32°C as required. For the CRISPR-Cas9 screen we used the HD_CFD sgRNA library, which are available from the Vienna Drosophila Resource Center (VDRC) (Port et al., 2020). For a full list of all screened lines, see Supplementary Table S1. The HD_CFD lines, containing the gRNAs, were crossed to a master stock line expressing Cas9 and two endogenously tagged read-out genes: *w-; Wg::GFP, Dll::dTom; hh-Gal4,UAS-Cas9uM/TM6b*. Other driver lines used in this study were *w-; ; Gal4-pdm2,UAS-Cas9uM/TM6b* and *w-; ; hh-Gal4,UAS-Cas9uM/TM6b*. Stocks obtained from the Bloomington *Drosophila* Stock Center, BDSC (NIH P40OD018537) were used in this study. The following fly lines were obtained from BDSC: gRNA Vps15 (BDSC #83822), gRNA Atg6 (BDSC #80830), gRNA Vps34 (BDSC#92484), UAS Vps15 RNAi (BDSC #34029), UAS Vps15 RNAi (BDSC #57011), UAS Vps15 RNAi (BDSC #35209), UAS Atg6 RNAi (BDSC #102460), UAS Vps34 RNAi (BDSC #33384) and UAS Vps34 RNAi (BDSC #36056).

Antibodies

For immunohistochemistry, the following primary antibodies were used: mouse anti-Wg (4D4, DSHB), 1:100 for immunofluorescence (IF) and 1:20 for extracellular staining; rabbit anti-Evi/Wls (Port et al., 2008), 1:800 for IF; guinea-pig anti-Sens (Gross et al., 2012), 1:300 for IF; 1:500 for IF; mouse anti-Dlg1 (4F3, DSHB), 1:50 for IF; mouse anti-Cnx99A (Cnx99A 6-2-1, DSHB), 1:5 for IF ; mouse anti-Golgin84 (Golgin84 12-1, DSHB), 1:5 for IF; rabbit anti-Rab5 (ab31261, Abcam), 1:500 for IF; mouse anti-Rab7 (Rab7, DSHB), 1:2 for IF; rabbit anti-Atg8 (ZRB1585, Sigma Aldrich), 1:50 for IF; rabbit anti-Arl8 (Arl8, DSHB), 1:200 for IF, FluoTag®-X4 anti-GFP conj. AbberiorStar635P (N0304-Ab635P, Abberior), 1:10 for the Wg uptake assay. As secondary antibodies (all in 1:800 dilution) we used goat anti-mouse Alexa Fluor 488 (A21202, Invitrogen), chicken anti-mouse Alexa Fluor 594 (A21201, Invitrogen), goat anti-mouse Alexa Fluor 647 (A21236, Invitrogen) with 1:200 for extracellular staining, goat anti-rabbit Alexa Fluor 488 (A11008, Invitrogen), goat anti-rabbit Alexa Fluor 647 (A21245, Invitrogen), goat anti-guinea pig Alexa Fluor 633 (A21105, Invitrogen), goat anti-rabbit STAR 635P (ST635P-1002, Abberior) or goat anti-mouse STAR 635P (ST635P-1001, Abberior) in 1:200 for STED microscopy. Imaginal discs were additionally stained with Hoechst33342 (H1399, Invitrogen) in 1:2000 dilution.

Immunohistochemistry

Imaginal wing discs of third instar larvae were dissected according to standard procedures. Wing discs were fixed with 4% formaldehyde (FA) in PBS for 20’ and washed several times with PBS-Triton 0.3%. For overnight incubation at 4°C with the primary antibody, the tissue was blocked using 1% normal goat serum in PBS. The fluorescently labelled secondary antibodies were applied on the next day after several washes with PBS-Triton 0.3%. For extracellular Wingless staining, larvae were kept for 15’ prior to dissection in ice cold Schneider’s medium with 4% FBS (SchM+) and subsequently dissected on ice in SchM+. Staining was performed with incubation on ice for 90’, with the primary antibody (1:20; Wg, 4D4) in SchM+. Discs were washed and fixed with 4% FA in SchM+ on ice for 40’, followed by another 10’ at room temperature. The Wg uptake

assay was based on (Witte et al., 2021). Wing discs were dissected at room temperature in SchM+ and incubated in primary antibody (1:20; Wg, 4D4) for 90', similarly to extracellular staining. Acid wash was done with 0.1mM Glycine with HCl (pH 3.5) for 5' and the discs were stringently washed with SchM+ (5 times, 3-5'). After the wash, discs were fixed for 20' at room temperature in 4% FA in SchM+. Treatment after fixation was similar to normal antibody staining for both the extracellular staining and the Wg uptake assay, using the secondary antibody in 1:200 dilution. All dissected discs were finally mounted in the anti-fade mounting medium Vectashield (VectorLabs) and placed on a Poly-L-Lysin (Roth) covered cover slip.

Fluorescent in situ hybridisation (FISH)

For *in situ* hybridisation, L3 wing imaginal discs were dissected in 1x PBS and fixed for 2x 20 min in 4% FA in PBS or PBS-T (1x PBS + 0.1% Triton X100), respectively. Tissues were hybridised at 65°C overnight with DIG-labelled *wg* antisense probe in hybridisation buffer HybA (50% formamide, 5x SSC pH 7.0, 10 mg/ml salmon sperm, 1 mg/ml tRNA, 100 µg/ml heparin and 0.2% Triton X100, adjust pH 6.5 with 1M HCl). *In situ* antisense probes were generated using a two-step PCR based method with the *wg* specific primers forward 5'CTCCCGGGAATTCGTCGATA, reverse 5'TTTTGGTCCGACACAGCTTG and a universal 3' T7 primer agggatcctaatacgactcactatagggcccggggc. Probes were transcribed with RNA T7 polymerase and labelled with the DIG RNA labelling mix (Roche). After hybridisation, tissues were washed with 1x PBS-T and blocked with 1x blocking reagent (Roche) in 1x Maleic acid buffer (100mM Maleic acid, 150mM NaCl, pH7.5). Samples were incubated overnight with the HRP-conjugated anti-DIG antibody (1:2000, Jackson, AB_2339011) in 1 x blocking reagent (Roche). For fluorescent signal detection samples were incubated with 1:50 TSA amplification diluent (PerkinElmer Life Sciences) and CF555 conjugated tyramide (Biotium Inc.) for reaction with HRP-conjugated antibody. Wing discs were mounted on Poly-L-Lysin (Sigma) coated coverslips and embedded in VectaShield antifade mounting medium (VectorLabs).

Light Microscopy and Super resolution microscopy

Wing discs were imaged using either a Leica TCS SP8 confocal microscope (Leica Microsystems) or a Zeiss LSM 900 Airyscan system (Carl Zeiss Microscopy GmbH), equipped with 40×/1.30 HC PL APO CS2 (oil) and 63×/1.40 (oil) objectives, respectively. Brightfield images of adult wings were acquired using a Zeiss Cell Observer.Z1 microscope with a 20×/0.8 Plan Apo DICII objective. These images were captured using an AxioCam MRm monochrome CCD camera (Carl Zeiss Microscopy GmbH). 3D STED super resolution images were acquired with near isotropic resolution as XZ-scans with a Leica Stellaris 8 STED Falcon microscope (Leica Microsystems). Imaginal discs were prepared and mounted in 1xPBS on a Poly-L-Lysin (Sigma) covered µ-Dish (35mm) with a high 1.5H glass coverslip bottom (#81158, Ibidi) and covered with 1.5H round (∅12mm) coverslips (Marienfeld). Imaging was performed with a HC PL APO 86x/1.20 W motCORR STED white objective (Leica Microsystems) at a pixel size of 0.04µm. The Wg::GFP was immuno-stained with a rabbit anti-GFP (Invitrogen) antibody and a goat anti-rabbit STAR 635P (Abberior) secondary antibody. The fluorophore Abberior Star635P was excited at 620nm. Depletion was performed with a 775nm STED laser. For the “Wg uptake” assay, the following settings were applied: eGFP was detected in confocal mode with 480nm laser excitation and an emission window ranging from 495nm to 550nm. The endogenous tagged Wg with GFP was detected using the FluoTag®-X4 anti-GFP conj. AbberiorStar635P (N0304-Ab635P, Abberior) and imaged in confocal and 3D-STED mode using 620nm laser excitation. Depletion in the STED channel was performed with a 775nm STED laser. The fluorescence was collected using a 635nm to 740nm detection window.

Data processing

Image data was processed and analysed using Fiji ImageJ suit Version 2.1.0/1.53c (Schindelin et al., 2012). Further analysis and data visualisation was performed using RStudio Version 2023.06.1+524 (R Core Team (2023), R: A Language and Environment for Statistical Computing, R Foundation for Statistical Computing, Vienna, Austria; RStudio Team (2020), RStudio: Integrated Development for R, RStudio, PBC, Boston, MA). All fluorescence intensity measurements were normalized to the intensity values in the leftmost 30nm per sample and plotted with the ggplot2 packages in R (Wickham,

2016). Figures with images and schematic drawings were created using Affinity Designer Version 1.10.8 (Serif). The summary statement was summarized by the artifical inteligence tool ChatGTP (OpenAI).

Acknowledgements

Research in the group of M.B. is supported by the Deutsche Forschungsgemeinschaft Collaborative Research Center CRC/SFB1324 Projects A01 (project number 331351713) on Mechanisms and Functions of Wnt signalling. The authors thank the Wnt CRC Consortium for the numerous stimulating discussions and exchanges. We would like to thank the DKFZ light microscopy core facility (LMCF) for their expertise and support. We thank Dominique Kranz for comments and discussion on the manuscript.

Competing interests

No competing interest declared.

Funding

Research in the group of M.B. is supported by the Deutsche Forschungsgemeinschaft Collaborative Research Center CRC/SFB1324 on Mechanisms and Functions of Wnt signalling (project number 331351713).

Data and resource availability

All relevant data and details of resources can be found within the article and its supplementary information.

References

Abe, M., Setoguchi, Y., Tanaka, T., Awano, W., Takahashi, K., Ueda, R., Nakamura, A. and Goto, S. (2009). Membrane Protein Location-Dependent Regulation by PI3K (III) and Rabenosyn-5 in Drosophila Wing Cells. *PLoS ONE* **4**, e7306.

Allen, S. E., Koreman, G. T., Sarkar, A., Wang, B., Wolfner, M. F. and Han, C. (2021). Versatile CRISPR/Cas9-mediated mosaic analysis by gRNA-induced crossing-over for unmodified genomes. *PLOS Biology* **19**, e3001061.

Alvarez-Rodrigo, I., Willnow, D. and Vincent, J.-P. (2023). The logistics of Wnt production and delivery. In *Current Topics in Developmental Biology*, pp. 1–60. Elsevier.

Backer, J. M. (2000). Phosphoinositide 3-Kinases and the Regulation of Vesicular Trafficking. *Molecular Cell Biology Research Communications* **3**, 193–204.

Backer, J. M. (2008). The regulation and function of Class III PI3Ks: novel roles for Vps34. *Biochemical Journal* **410**, 1–17.

Baker, N. E. (2024). Founding the Wnt gene family: How *wingless* was found to be a positional signal and oncogene homolog. *BioEssays* **46**, 2300156.

Balla, T. (2013). Phosphoinositides: Tiny Lipids With Giant Impact on Cell Regulation. *Physiological Reviews* **93**, 1019–1137.

Bänziger, C., Soldini, D., Schütt, C., Zipperlen, P., Hausmann, G. and Basler, K. (2006). Wntless, a conserved membrane protein dedicated to the secretion of Wnt proteins from signaling cells. *Cell* **125**, 509–22.

Bartscherer, K., Pelte, N., Ingelfinger, D. and Boutros, M. (2006). Secretion of Wnt Ligands Requires Evi, a Conserved Transmembrane Protein. *Cell* **125**, 523–533.

Beckett, K., Monier, S., Palmer, L., Alexandre, C., Green, H., Bonneil, E., Raposo, G., Thibault, P., Le Borgne, R. and Vincent, J. P. (2013). Drosophila S2 cells secrete wingless on exosome-like vesicles but the wingless gradient forms independently of exosomes. *Traffic* **14**, 82–96.

Brunner, E., Yagi, R., Debrunner, M., Beck-Schneider, D., Burger, A., Escher, E., Mosimann, C., Hausmann, G. and Basler, K. (2019). CRISPR-induced double-strand breaks trigger recombination between homologous chromosome arms. *Life Sci Alliance* **2**, e201800267.

Brunt, L. and Scholpp, S. (2018). The function of endocytosis in Wnt signaling. *Cell Mol Life Sci* **75**, 785–795.

Chandra, M., Chin, Y. K.-Y., Mas, C., Feathers, J. R., Paul, B., Datta, S., Chen, K.-E., Jia, X., Yang, Z., Norwood, S. J., et al. (2019). Classification of the human phox

homology (PX) domains based on their phosphoinositide binding specificities. *Nat Commun* **10**, 1528.

Chaudhary, V. and Boutros, M. (2019). Exocyst-mediated apical Wg secretion activates signaling in the Drosophila wing epithelium. *PLoS Genet* **15**, e1008351.

Chaudhary, V., Hingole, S., Frei, J., Port, F., Strutt, D. and Boutros, M. (2019). Robust Wnt signaling is maintained by a Wg protein gradient and Fz2 receptor activity in the developing Drosophila wing. *Development* **146**,.

Clevers, H. and Nusse, R. (2012). Wnt/β-Catenin Signaling and Disease. *Cell* **149**, 1192–1205.

Coombs, G. S., Yu, J., Canning, C. A., Veltri, C. A., Covey, T. M., Cheong, J. K., Utomo, V., Banerjee, N., Zhang, Z. H., Jadulco, R. C., et al. (2010). WLS-dependent secretion of WNT3A requires Ser209 acylation and vacuolar acidification. *J. Cell Sci.* **123**, 3357–3367.

Evron, T., Caspi, M., Kazelnik, M., Shor-Nareznoy, Y., Armoza-Eilat, S., Kariv, R., Manber, Z., Elkon, R., Sklan, E. H. and Rosin-Arbesfeld, R. (2021). A CRISPR knockout screen reveals new regulators of canonical Wnt signaling. *Oncogenesis* **10**, 63.

Goodman, R. M., Thombre, S., Firtina, Z., Gray, D., Betts, D., Roebuck, J., Spana, E. P. and Selva, E. M. (2006). Sprinter: a novel transmembrane protein required for Wg secretion and signaling. *Development* **133**, 4901–11.

Grobe, K. and Guerrero, I. (2020). Dally-like Is Unlike Dally in Assisting Wingless Spread. *Developmental Cell* **54**, 572–573.

Gross, J. C. (2021). Extracellular WNTs: Trafficking, Exosomes, and Ligand–Receptor Interaction. *Handb Exp Pharmacol.* **269**, 29–43.

Gross, J. C., Chaudhary, V., Bartscherer, K. and Boutros, M. (2012). Active Wnt proteins are secreted on exosomes. *Nat Cell Biol.* **14**, 1036–1045.

Han, C., Yan, D., Belenkaya, T. Y. and Lin, X. (2005). Drosophila glypicans Dally and Dally-like shape the extracellular Wingless morphogen gradient in the wing disc. *Development* **132**, 667–679.

Hayakawa, A., Hayes, S. J., Lawe, D. C., Sudharshan, E., Tuft, R., Fogarty, K., Lambright, D. and Corvera, S. (2004). Structural Basis for Endosomal Targeting by FYVE Domains. *Journal of Biological Chemistry* **279**, 5958–5966.

Hemalatha, A., Prabhakara, C. and Mayor, S. (2016). Endocytosis of Wingless via a dynamin-independent pathway is necessary for signaling in Drosophila wing discs. *Proceedings of the National Academy of Sciences* **113**, E6993–E7002.

Holstein, T. W. (2012). The Evolution of the Wnt Pathway. *Cold Spring Harb Perspect Biol* **4**,.

Holzem, M., Boutros, M. and Holstein, T. W. (2024). The origin and evolution of Wnt signalling. *Nat Rev Genet* **25**, 500–512.

Hurley, J. (2006). Membrane binding domains. *Biochimica et Biophysica Acta (BBA) - Molecular and Cell Biology of Lipids* **1761**, 805–811.

Jenny, F. H. and Basler, K. (2014). Powerful Drosophila screens that paved the wingless pathway. *Fly (Austin)* **8**, 218–25.

Khare, N. and Baumgartner, S. (2000). Dally-like protein, a new Drosophila glypican with expression overlapping with wingless. *Mechanisms of Development* **99**, 199–202.

Kramps, T., Peter, O., Brunner, E., Nellen, D., Froesch, B., Chatterjee, S., Murone, M., Züllig, S. and Basler, K. (2002). Wnt/Wingless Signaling Requires BCL9/Legless-Mediated Recruitment of Pygopus to the Nuclear β-Catenin-TCF Complex. *Cell* **109**, 47–60.

Lemmon, M. A. (2003). Phosphoinositide Recognition Domains. *Traffic* **4**, 201–213.

Lindmo, K. and Stenmark, H. (2006). Regulation of membrane traffic by phosphoinositide 3-kinases. *Journal of Cell Science* **119**, 605–614.

Loh, K. M., van Amerongen, R. and Nusse, R. (2016). Generating Cellular Diversity and Spatial Form: Wnt Signaling and the Evolution of Multicellular Animals. *Dev. Cell* **38**, 643–655.

Lőrincz, P., Lakatos, Z., Maruzs, T., Szatmári, Z., Kis, V. and Sass, M. (2014). Atg6/UVRAG/Vps34-Containing Lipid Kinase Complex Is Required for Receptor Downregulation through Endolysosomal Degradation and Epithelial Polarity during *Drosophila* Wing Development. *BioMed Research International* **2014**, 1–19.

Mills, I. G., Jones, A. T. and Clague, M. J. (1998). Involvement of the endosomal autoantigen EEA1 in homotypic fusion of early endosomes. *Current Biology* **8**, 881–884.

Mittermeier, L. and Virshup, D. M. (2022). An itch for things remote: The journey of Wnts. *Curr Top Dev Biol.* **150**, 91–128.

Moti, N., Yu, J., Boncompain, G., Perez, F. and Virshup, D. M. (2019). Wnt traffic from endoplasmic reticulum to filopodia. *PLoS One* **14**, e0212711.

Niehrs, C. (2012). The complex world of WNT receptor signalling. *Nat Rev Mol Cell Biol* **13**, 767–779.

Nüsslein-Volhard, C., Wieschaus, E. and Kluding, H. (1984). Mutations affecting the pattern of the larval cuticle inDrosophila melanogaster: I. Zygotic loci on the second chromosome. *Wilhelm Roux' Archiv* **193**, 267–282.

Panaretou, C., Domin, J., Cockcroft, S. and Waterfield, M. D. (1997). Characterization of p150, an Adaptor Protein for the Human Phosphatidylinositol (PtdIns) 3-Kinase. *Journal of Biological Chemistry* **272**, 2477–2485.

Port, F. and Boutros, M. (2022). Tissue-Specific CRISPR-Cas9 Screening in Drosophila. *Methods Mol Biol* **2540**, 157–176.

Port, F., Kuster, M., Herr, P., Furger, E., Banziger, C., Hausmann, G. and Basler, K. (2008). Wingless secretion promotes and requires retromer-dependent cycling of Wntless. *Nat Cell Biol* **10**, 178–85.

Port, F., Hausmann, G. and Basler, K. (2011). A genome-wide RNA interference screen uncovers two p24 proteins as regulators of Wingless secretion. *EMBO Rep* **12**, 1144–52.

Port, F., Chen, H.-M., Lee, T. and Bullock, S. L. (2014). Optimized CRISPR/Cas tools for efficient germline and somatic genome engineering in *Drosophila*. *Proc. Natl. Acad. Sci. U.S.A.* **111**,.

Port, F., Strein, C., Stricker, M., Rauscher, B., Heigwer, F., Zhou, J., Beyersdörffer, C., Frei, J., Hess, A., Kern, K., et al. (2020). A large-scale resource for tissue-specific CRISPR mutagenesis in Drosophila. *Elife* **9**,.

Rim, E. Y., Clevers, H. and Nusse, R. (2022). The Wnt Pathway: From Signaling Mechanisms to Synthetic Modulators. *Annual Review of Biochemistry* **91**, 571–598.

Routledge, D. and Scholpp, S. (2019). Mechanisms of intercellular Wnt transport. *Development* **146**, dev176073.

Rusten, T. E., Lindmo, K., Juhász, G., Sass, M., Seglen, P. O., Brech, A. and Stenmark, H. (2004). Programmed Autophagy in the Drosophila Fat Body Is Induced by Ecdysone through Regulation of the PI3K Pathway. *Developmental Cell* **7**, 179–192.

Schindelin, J., Arganda-Carreras, I., Frise, E., Kaynig, V., Longair, M., Pietzsch, T., Preibisch, S., Rueden, C., Saalfeld, S., Schmid, B., et al. (2012). Fiji: an open-source platform for biological-image analysis. *Nature methods* **9**, 676–82.

Sharma, S. and Chaudhary, V. (2024). Dissociation of Drosophila Evi-Wg Complex Occurs Post Apical Internalization in the Maturing Acidic Endosomes. *Traffic* **25**, e12955.

Shravage, B. V., Hill, J. H., Powers, C. M., Wu, L. and Baehrecke, E. H. (2013). *Atg6* is required for multiple vesicle trafficking pathways and hematopoiesis in *Drosophila*. *Development* **140**, 1321–1329.

Simonsen, A., Lippe, R., Christoforidis, S., Gaullier, J.-M., Brech, A., Callaghan, J., Toh, B.-H., Murphy, C., Zerial, M. and Stenmark, H. (1998). EEA1 links PI(3)K function to Rab5 regulation of endosome fusion. *Nature* **394**, 494–498.

Stanganello, E. and Scholpp, S. (2016). Role of cytonemes in Wnt transport. *J Cell Sci* **129**, 665–72.

Stanganello, E., Hagemann, A. I., Mattes, B., Sinner, C., Meyen, D., Weber, S., Schug, A., Raz, E. and Scholpp, S. (2015). Filopodia-based Wnt transport during vertebrate tissue patterning. *Nat Commun* **6**, 5846.

Stenmark, H., Aasland, R., Toh, B.-H. and D'Arrigo, A. (1996). Endosomal Localization of the Autoantigen EEA1 Is Mediated by a Zinc-binding FYVE Finger. *Journal of Biological Chemistry* **271**, 24048–24054.

Strigini, M. and Cohen, S. M. (1999). Formation of morphogen gradients in the Drosophila wing. *Semin Cell Dev Biol* **10**, 335–44.

Swarup, S. and Verheyen, E. M. (2012). Wnt/Wingless signaling in Drosophila. *Cold Spring Harb Perspect Biol* **4**,.

Swarup, S., Pradhan-Sundd, T. and Verheyen, E. M. (2015). Genome-wide identification of phospho-regulators of Wnt signaling in Drosophila. *Development* **142**, 1502–1515.

Tuma, P. L., Nyasae, L. K., Backer, J. M. and Hubbard, A. L. (2001). Vps34p differentially regulates endocytosis from the apical and basolateral domains in polarized hepatic cells. *The Journal of Cell Biology* **154**, 1197–1208.

Waghmare, I., Wang, X. and Page-McCaw, A. (2020). Dally-like protein sequesters multiple Wnt ligands in the Drosophila germarium. *Developmental Biology* **464**, 88–102.

Wickham, H. (2016). ggplot2: Elegant Graphics for Data Analysis. *Springer-Verlag New York*.

Widmann, T. J. and Dahmann, C. (2009). Wingless signaling and the control of cell shape in Drosophila wing imaginal discs. *Developmental Biology* **334**, 161–173.

Wiese, K. E., Nusse, R. and van Amerongen, R. (2018). Wnt signalling: conquering complexity. *Development* **145**, dev165902.

Witte, L., Linnemannstöns, K., Honemann-Capito, M. and Gross, J. (2021). Visualization and Quantitation of Wg trafficking in the Drosophila Wing Imaginal Epithelium. *BIO-PROTOCOL* **11**,.

Wolf, L. and Boutros, M. (2023). The role of Evi/Wntless in exporting Wnt proteins. *Development* **150**, dev201352.

Wu, J., Randle, K. E. and Wu, L. P. (2007). ird1 is a Vps15 homologue important for antibacterial immune responses in Drosophila. *Cell Microbiol* **9**, 1073–1085.

Wurmser, A. E., Gary, J. D. and Emr, S. D. (1999). Phosphoinositide 3-Kinases and Their FYVE Domain-containing Effectors as Regulators of Vacuolar/Lysosomal Membrane Trafficking Pathways. *Journal of Biological Chemistry* **274**, 9129–9132.

Yan, D., Wu, Y., Feng, Y., Lin, S.-C. and Lin, X. (2009). The Core Protein of Glypican Dally-Like Determines Its Biphasic Activity in Wingless Morphogen Signaling. *Developmental Cell* **17**, 470–481.

Figures

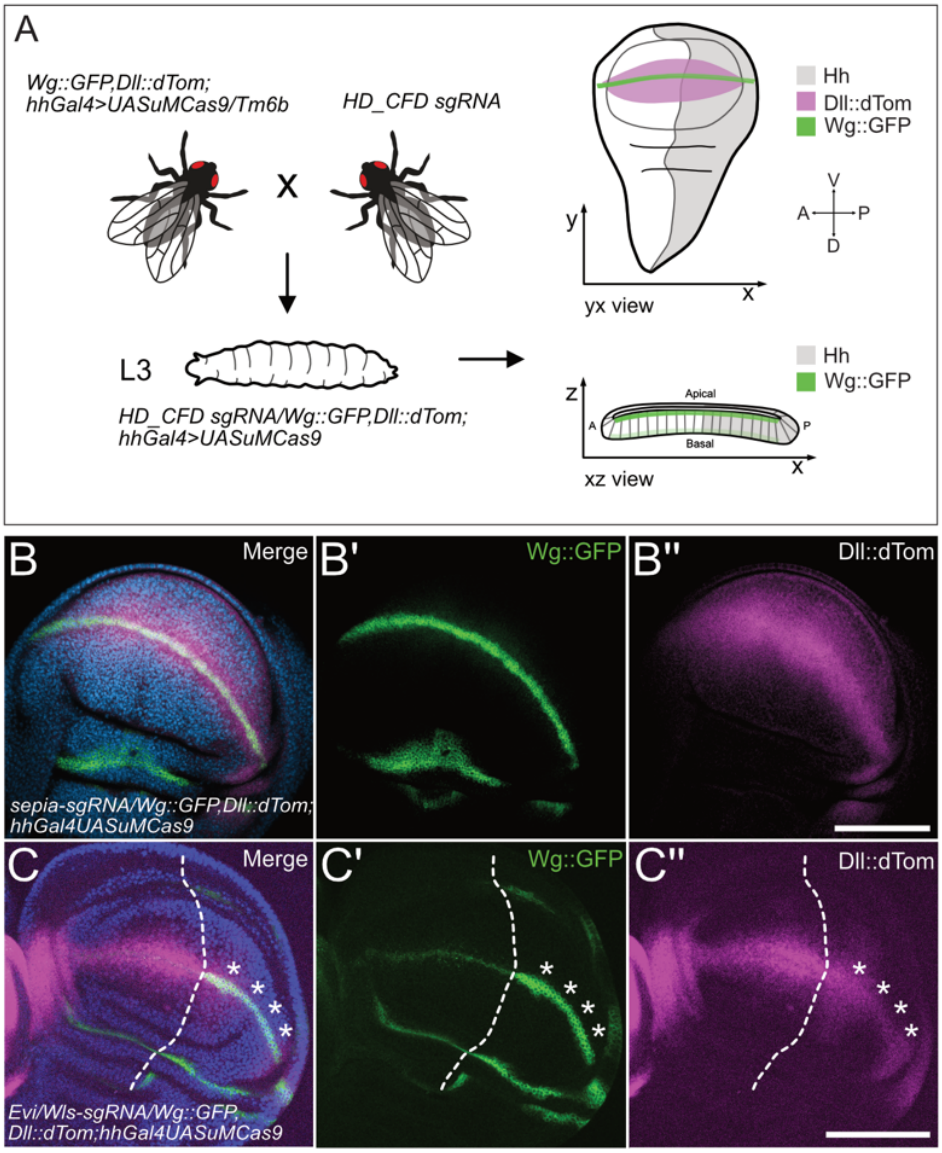

Figure 1 | Screening for novel candidates of Wg secretion in the developing *Drosophila* wing epithelium. (A) Overview of the screening procedure. The driver line *w-;Wg::GFP,Dll::dTom;hh-Gal4, UAS-Cas9uM/TM6b* was crossed to the sgRNA containing HD_CFD fly lines. Third instar larvae (wandering stage) were dissected and wing imaginal discs were mounted for confocal analysis. Indicated are also the used orientation of the wing imaginal disc, the xy and xz view. Expression patterns of Wg::GFP (green), Dll::dTom (magenta) and Hh (gray) are indicated schematically. (B-B'') Confocal imaging of the negative control *sepia-sgRNA* with the endogenous labelled (B') Wg::GFP (green) and (B'') Dll::dTom (magenta) pattern. No differences in fluorescence signal are detected in the anterior or posterior compartment. (C-C'') Confocal imaging of the positive control line *Evi/Wls-sgRNA* showing a strong increase of (C') Wg::GFP at the DV boundary (asterisks), and (C'') a loss of Dll::dTom in the corresponding area. The dashed line indicates the border between the anterior and posterior compartment. Presented

confocal images are average intensity projections for both genotypes. All nuclei are stained with Hoechst33342 (blue). Confocal images were taken with the 40x oil objective. Scale bar = 100um. A; Anterior; D: Dorsal; dTom: dTomato; GFP: Green fluorescent protein; Hh: Hedgehog; P: Posterior; Se: Sepia; UAS: Upstream activation sequence; V: Ventral.

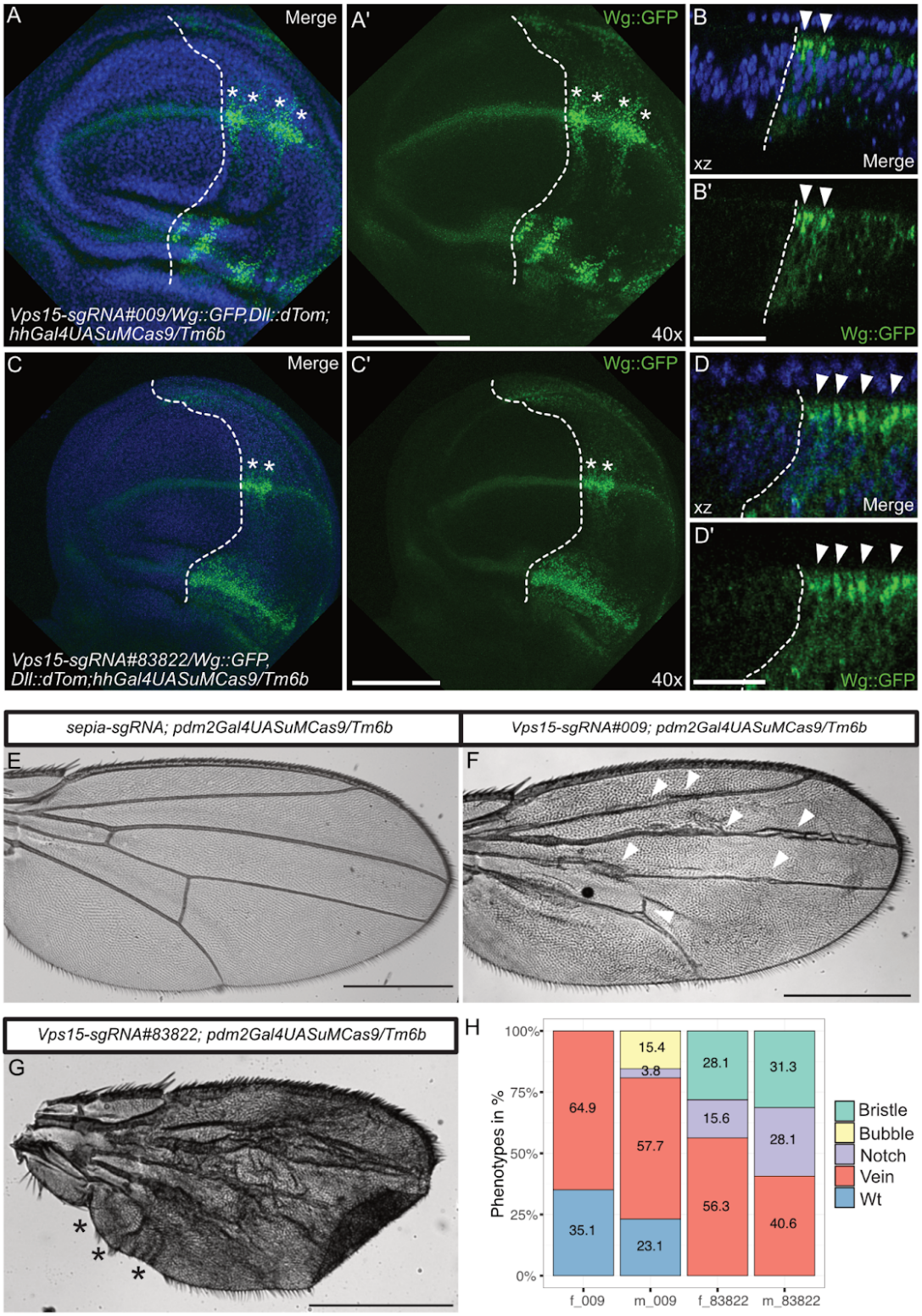

Figure 2 | Characterisation of Vps15 mutagenesis in *Drosophila*. (A,A') Wg protein abundance at the DV boundary in the wing discs of larvae of the cross *w-;Wg::GFP,Dll:dTom;hh-Gal4,UASCas9uM/Tm6B* with the HD_CFD *Vps15-sgRNA#009* fly line. The perturbed posterior area of the wing disc is indicated by the dashed line. Genetic mosaics with Vps15 mutagenesis are labelled

by white asterisks. (B,B') The Wg protein accumulation in the xz view shows its location at the apical membrane (arrowheads) and its spreading towards the basal side of the cell. (C,C') Wg phenotype of the BDSC *Vps15-sgRNA#83822* fly line crossed with *w-;Wg::GFP,Dll:dTom;hh-Gal4,UASCas9uM/Tm6B*. Strong accumulation can also be detected at the DV boundary (asterisks) and (D,D') at the apical membrane in the xz view (indicated with arrowheads). (A-D') All confocal images were taken with the 63x oil objective. Nuclei were stained with Hoechst33342 (blue). All discs are orientated with the wildtype tissue towards the left (anterior) and perturbed tissue towards the right (posterior). Confocal images are maximum intensity projections for both genotypes. (A,C) Scale bar = 100um. (B,D) Scale bar = 50um. (E-G) Adult wings of crosses with the *w-;;pdm2-Gal4,UASCas9uM/Tm6B* with (E) *sepia-sgRNA* as a negative control indicating the wildtype wing and (F) with *Vps15-sgRNA#009* or (G) *Vps15-sgRNA#838322* showing the perturbed wing tissue. (F) *Vps15-sgRNA#009* perturbed wings show a vein phenotype (white arrowheads). Further phenotypes observed include bubbles or notches, both also combined with vein phenotypes (Pictures not shown). (G) Wings with *Vps15-sgRNA#83822* perturbations show a more drastic phenotype than wings in (F). All wing tissue is highly disrupted while notches (black asterisks) and bristle phenotypes are observed regularly. Scale bar = 500um. (H) Distribution of wing phenotypes in *Vps-sgRNA#009* female (n_{female}=37), male (n_{male}=26) and *Vps15-sgRNA#83822* female (n_{female}=32), male (n_{male}=32) mutated flies. In *Vps15-sgRNA#009* flies wildtype wings were observed in female and male samples, while most wings show a vein phenotype. In male wings, also notches and bubbles occurred. No wildtype wings occurred in *Vps15-sgRNA#83822* female and male samples. All wings are disrupted and show a vein phenotype. Additionally notches and loss of bristles are observed in both genders. Numbers within the coloured bars indicate percentages of each corresponding phenotype. dTom: dTomato; f = female; GFP: Green fluorescent protein; Hh: Hedgehog; m = male; pdm2: POU domain protein 2; Wt: wildtype; UAS: Upstream Activation Sequence.

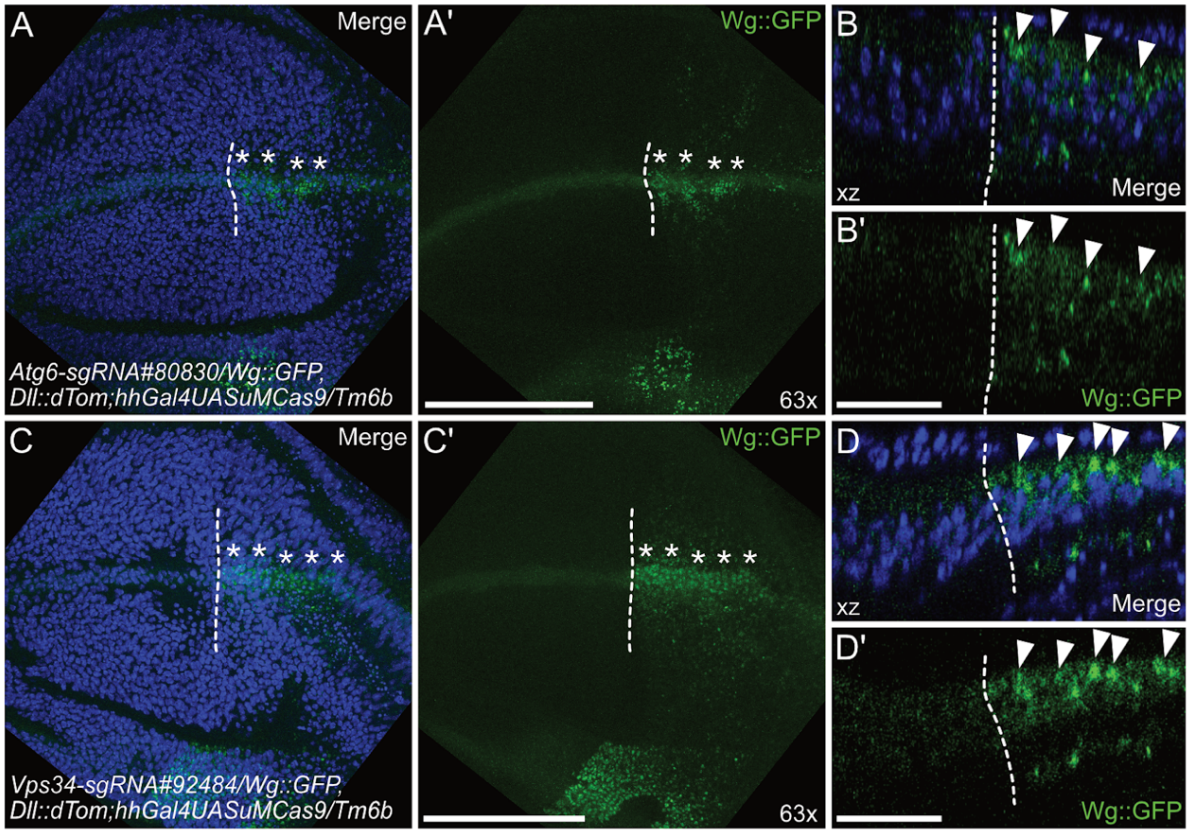

Figure 3 | Phenotypic characterisation of Atg6 and Vps34 mutagenesis in the wing imaginal disc. (A,A') Wg protein abundance at the DV boundary in the wing discs of larvae of the cross with *w-;Wg::GFP, Dll:dTom;hh-Gal4,UASCas9uM/Tm6B* with the BDSC Atg6-*sgRNA#80830* fly line. Atg6 mutagenesis shows accumulation of Wg protein at the DV boundary (asterisks). (B,B') Wg accumulation is also detected at the apical membrane in the xz view (arrowheads). (C,C') Wing imaginal disc of the cross of *w-;Wg::GFP,Dll:dTom;hh-Gal4,UASCas9uM/Tm6B* with the BDSC Vps34-*sgRNA#92484* shows accumulation of Wg::GFP at the DV boundary (asterisks). The loss of Vps34 phenocopies Atg6 and Vps15 phenotypes. Wg protein accumulation at the DV boundary can be detected and (D,D') this Wg accumulation is also localised at the apical membrane, while also spreading towards the basal side (arrowheads). All confocal images were taken with the 63x oil objective. Nuclei were stained with Hoechst33342 (blue). All discs are orientated with the wildtype tissue towards the left (anterior) and perturbed tissue towards the right (posterior). If possible, borders between both regions are indicated with white dashed lines. Presented are maximum intensity projections for all panels. (A,C) Scale bar = 100um. (B,D) Scale bar = 50um. dTom: dTomato; GFP: Green fluorescent protein; Hh: Hedgehog; UAS: Upstream Activation Sequence.

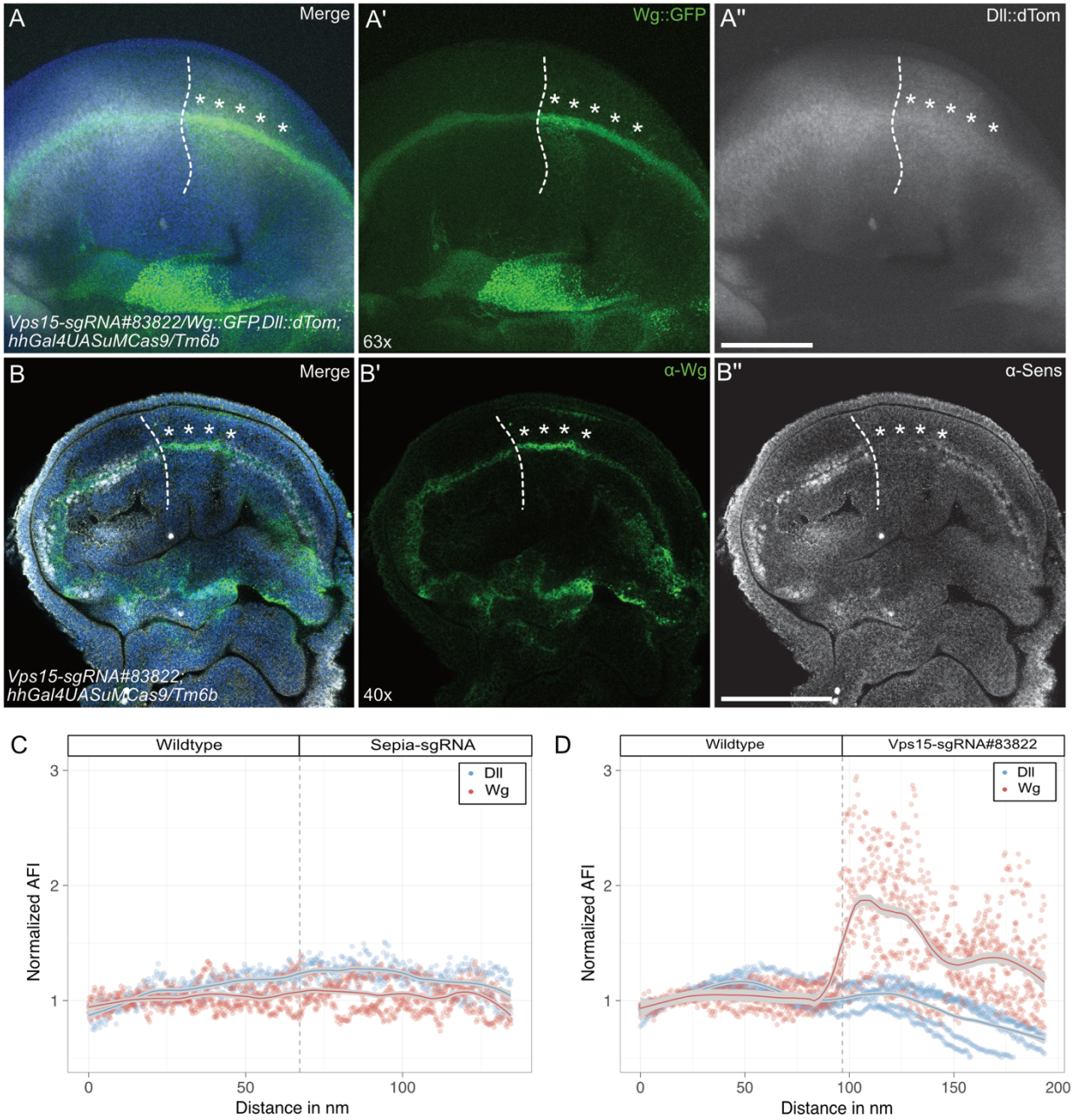

Figure 4 | Vps15 mutagenesis affects Wnt signalling. (A-A'') The Wnt signalling target Dll is slightly reduced in Vps15 (*w-;Vps15-sgRNA#83822/ Wg::GFP, Dll::dTom; hhGal4UasuMCas9/ Tm6b)* perturbed tissue (asterisks). The area of reduced Dll corresponds to the area of Wg accumulation. (B-B'') The Wnt target gene *sens* is also reduced (circled area) in Vps15 (*w-;Vps15-sgRNA#009/ Wg::GFP, Dll::dTom; hhGal4UasuMCas9/ Tm6b)* perturbed areas of wing discs. Magnifications of the perturbed area are shown at the right bottom corner. (C) Normalized fluorescence intensity measurements of Wg::GFP and Dll::dTom in the *w-;Sepia-sgRNA/Wg::GFP, Dll::dTom;hhGal4UasuMCas9/Tm6b* genetic background. The measurements represent a non-perturbed Wg::GFP (Red) and Dll::dTom (Blue) pattern. (D) In the *w-;Vps15-sgRNA#83822/ Wg::GFP, Dll::dTom; hhGal4UasuMCas9/ Tm6b* genetic background, Wg::GFP (Red) fluorescence is highly

increased in the posterior compartment, while Dll::dTom (Blue) fluorescence is reduced. Confocal images were taken with the 40x and 63x oil objective as indicated. Nuclei are stained with Hoechst33342 (blue). All discs are oriented with anterior towards the left and perturbed areas are marked with dashed lines. Presented are maximum intensity projections. Scale bars = 100um. AFI: Average fluorescence intensities; dTom: dTomato; GFP: Green fluorescent protein; Hh: Hedgehog; mut: mutated area; nm = nanometer; UAS: upstream Activation Sequence; Wt: Wildtype.

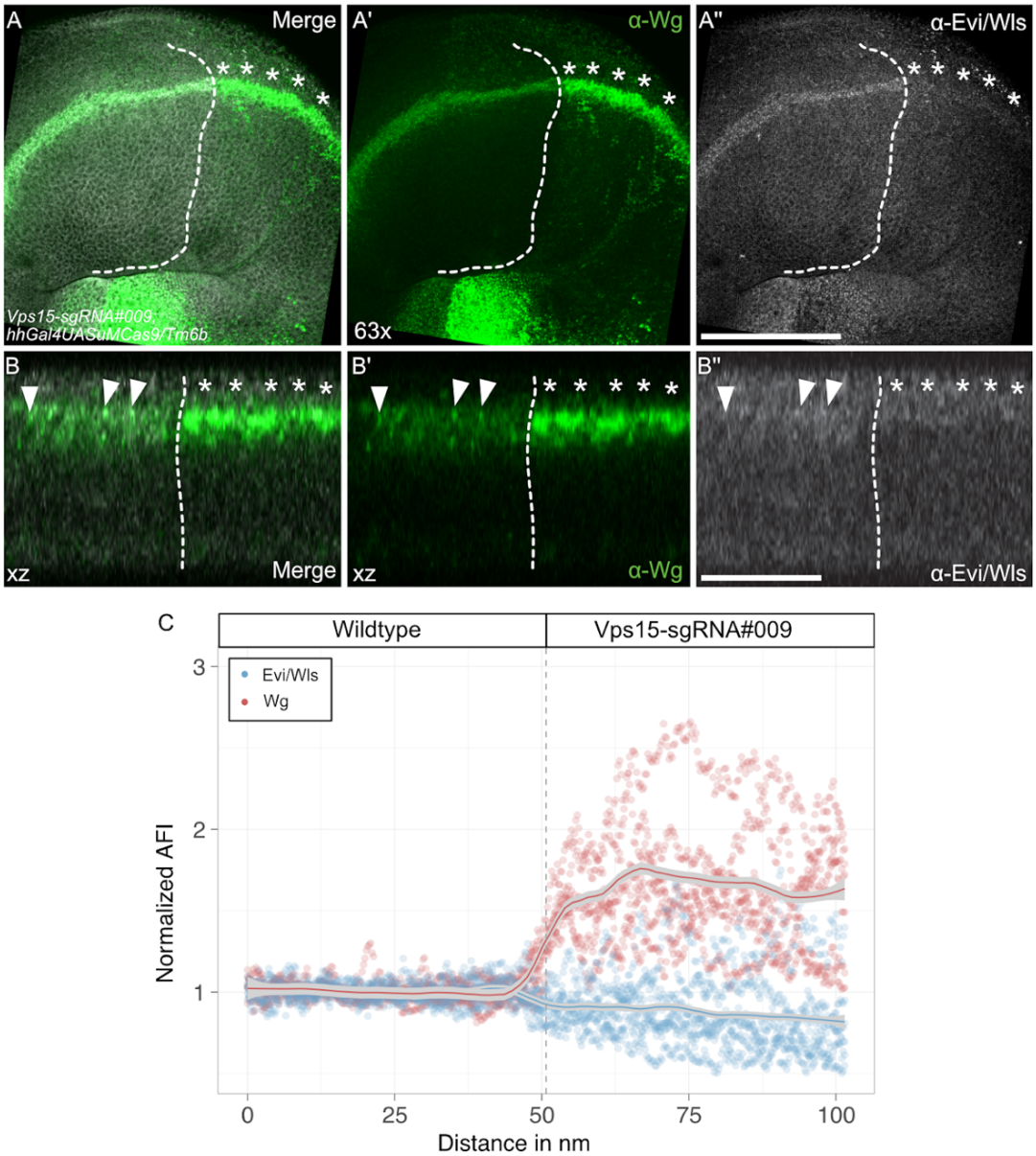

Figure 5 | Effects of Vps15 perturbation on Evi/Wls. (A-A'') Vps15 perturbation does not affect Evi/Wls protein despite Wg accumulation (arrowheads) (*w-;Vps15-sgRNA#83822; hhGal4UASuMCas9/ Tm6b*). (B-B'') This can also be observed in xz view in the same tissue (asterisks). Colocalization of Wg and Evi/Wls in the wildtype tissue is indicated with white arrow heads. The strong Wg accumulation at the apical membrane is indicated with asterisks. No accumulation of Evi/Wls is detectable in the perturbed tissue. (C) Average fluorescence intensity measurements of Wg::GFP (red) and Evi/Wls (blue) (n=6). Confocal images were taken with the 63x oil objective. All discs are oriented with anterior towards the left and perturbed areas are marked with dashed lines. Presented are maximum intensity projections. (A) Scale bars = 100um. (B) Scale bar = 50um. AFI: Average fluorescence intensities; dTom: dTomato; GFP: Green fluorescent protein; Hh: Hedgehog; mut: mutated area; nm = nanometer; UAS: upstream Activation Sequence; Wt: Wildtype.

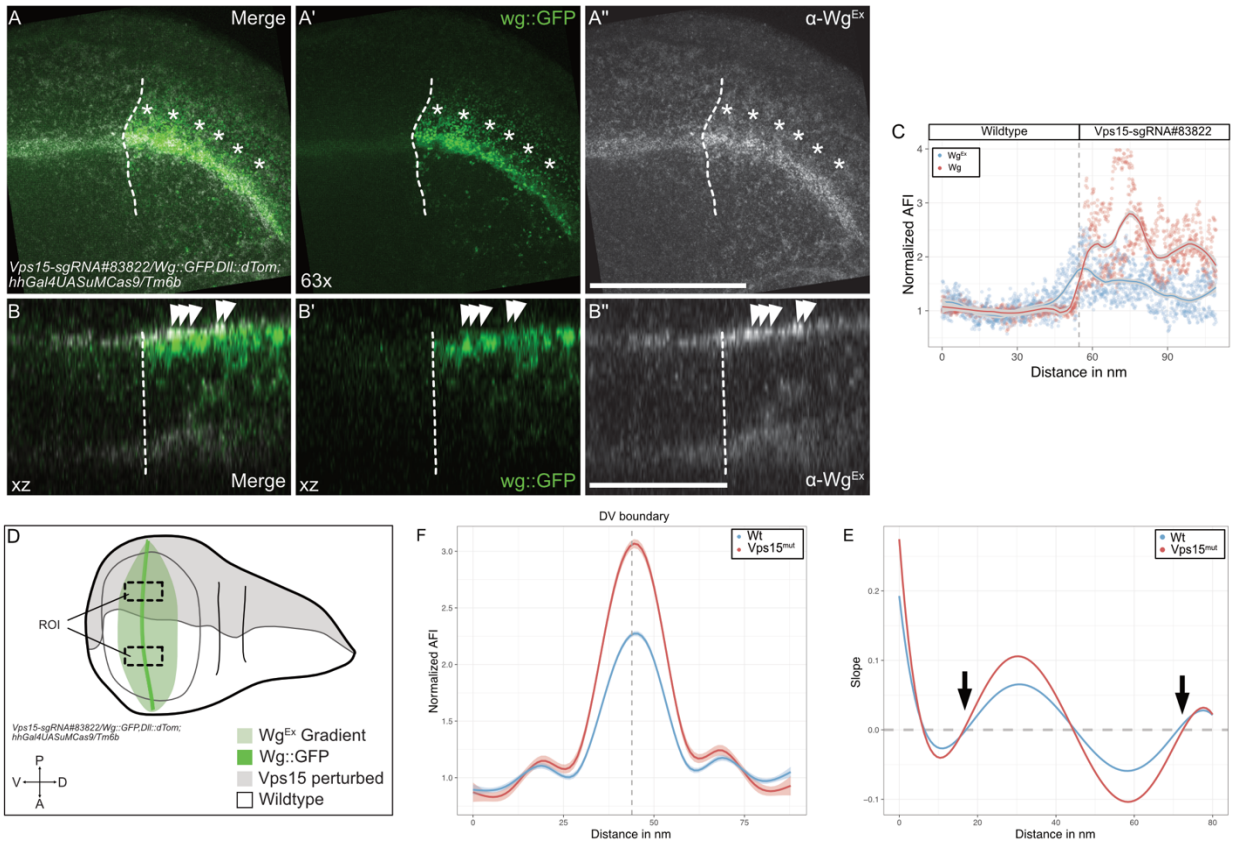

Figure 6 | Effects of Vps15 mutagenesis on extracellular Wg and gradient formation. (A-A'') Extracellular Wg (Wg^{Ex}) accumulates at the DV boundary in Vps15 mutated clones (asterisks; *w-; Vps15-sgRNA#83822/ Wg::GFP, Dll::dTom; hhGal4UASuMCas9/ Tm6b*). (B-B'') In the xz view, an apical accumulation of Wg^{Ex} can be detected in the Vps15 mutated cells, which is located above the endogenous Wg::GFP signal (white arrowheads). (C) The average fluorescence intensity is increased for Wg::GFP (Red) and Wg^{Ex} (blue) in the perturbed area. (D) Schematic of the gradient measurements. The same ROI was measured in the unperturbed and Vps15 perturbed tissue. The fluorescence intensity measurements of Wg^{Ex} indicate the range of the gradient in the tissue. (E) Average fluorescence intensity measurements of the Wg^{Ex} gradient in unperturbed (blue) and perturbed (red) tissue (n=16). (F) Derivative plot of the measuremnts in (E) show similar intersections (black arrows) of the two curves with the x-axis, indicating no differences in the Wg^{Ex} spreading. (A,B) All pictures are oriented with anterior to the left. The borders of the anterior and posterior area are indicated by a dashed line. Confocal images are taken with the 63x oil objective. Presented images are maximum intensity projections. (A) Scale bar = 100um. (B) Scale bar = 50um. AFI: Average fluorescence intensity; dTom: dTomato; DV: Dorsal-Ventral; GFP: Green fluorescent protein; Hh: Hedgehog; mut: mutated; nm: nanometer; ROI: Region of interest; UAS: Upstream Activation Sequence; Wt: Wildtype.

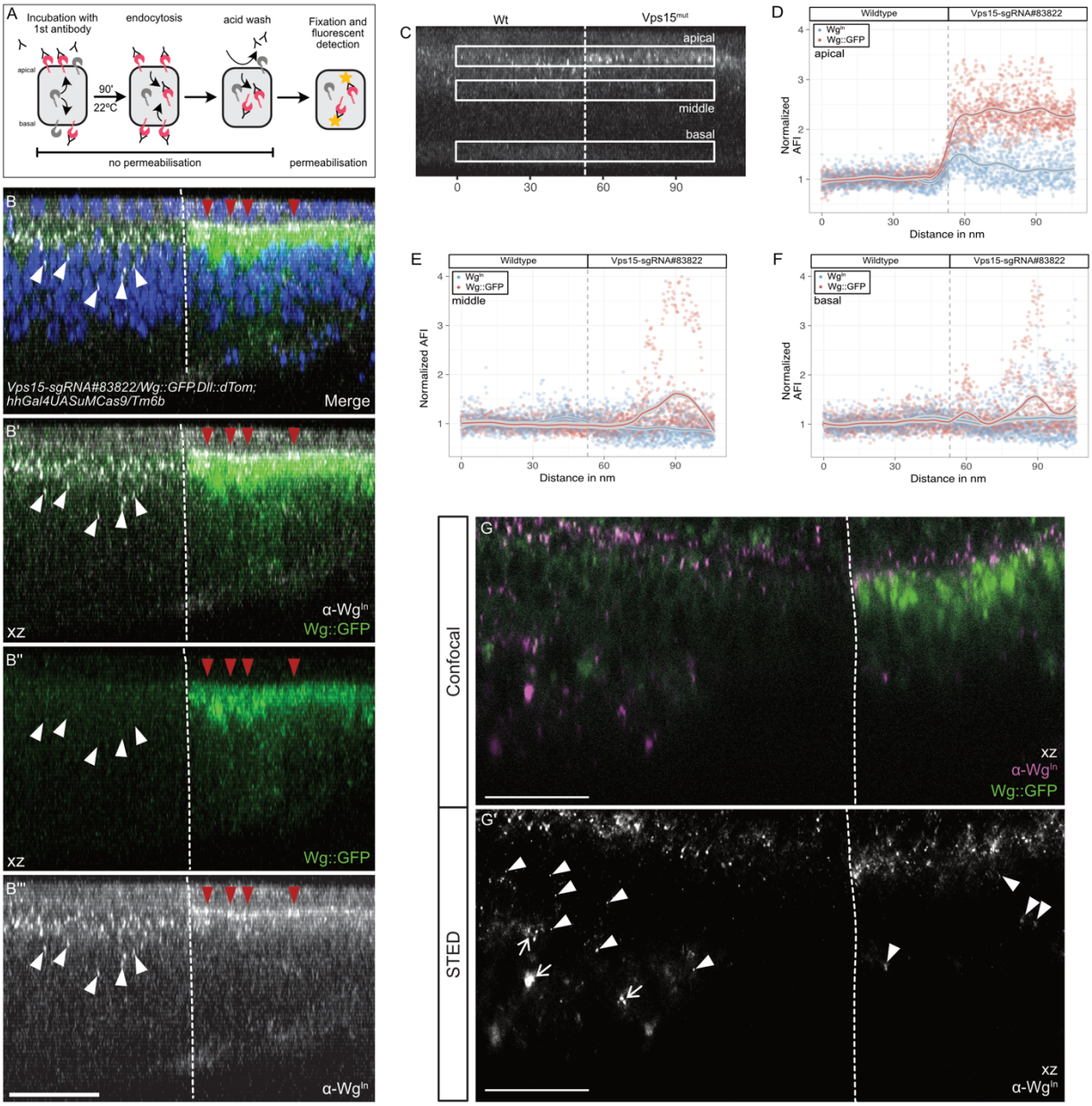

Figure 7 | The role of PI3K (III) in Wg endocytosis in *Drosophila* wing imaginal discs. (A) Schematic overview of the "Wg-uptake" assay (Witte et al., 2021). Wing discs are incubated at 22°C for 90' with the primary antibody to stain extracellular Wg and enabling re-endocytosis. Next, any extracellular primary antibodies are washed off with an acid wash. These steps were performed without any permeabilization. Then, wing discs were fixed and incubated with a fluorescent coupled secondary antibody to detect labelled Wg. Endocytosed and labeled Wg will be called Wg^{In} (B-B''') Representative image (n=10) of treated "Wg uptake" assay in wing imaginal discs. Here, we crossed the *w-;Wg::GFP,Dll:dTom; hh-Gal4UASCas9uM/ Tm6B* driver line with the Vps15-*sgRNA#83822* fly line. Shown is the xz view of the area of interest at the DV boundary, covering equal amounts of unperturbed and perturbed tissue. Unperturbed, anterior tissue is oriented to the left in all confocal images. The Hh border between these two compartments is indicated by a dashed line. Apical accumulation of Wg^{In} can be detected in Vps15 perturbed cells (red arrowheads) as seen in the

merged channels (B and B'). The fluorescence signal of Wg::GFP (B'') does partially overlap with the Wg^{In} signal (B''''). Wg^{In} dots in the intracellular area beneath the apical membrane are labelled with white arrowheads. (C) Schematic overview of the areas measured for fluorescence intensities: apical, middle and basal. (D) Normalised data for the fluorescence intensity analysis indicates an increase of Wg^{In} at the apical membrane (blue). The Area of Wg^{In} increase corresponds to the strong apical accumulation of the Wg::GFP signal (red). (E) Fluorescence intensity measurements of the middle area reveal a decrease of Wg^{In} in Vps15 perturbed tissue (blue), while the spreading of the Wg::GFP signal accumulation in the cytoplasm can be detected (red). (F) Fluorescence intensities at the basal membrane do not show a difference for the Wg^{In} signal (blue). (G-G') Super resolution microscopy of the Wg uptake assay in the Vps15 perturbed tissue. (G) Confocal images of the Wg::GFP (white) and Wg In (magenta) staining were merged and used as orientation. The dashed line divides the unperturbed (left) and perturbed (right) tissue. In (G') the Wg uptake assay is presented using super resolution microscopy. The image was taken with 3D STED in an xz view, for details see Material and Methods. Arrowheads indicate single Wg molecules, which are more frequently present in the unperturbed tissue. White arrows indicate large accumulations of Wg molecules, which might be located within cellular compartments. These accumulations are not observed in the Vps15 perturbed tissue. All confocal images are taken with the 63x oil objective. Nuclei are stained with Hoechst33342 (blue). Confocal images are maximum intensity projections. (B) Scale bar = 50um. (G) Scale bar = 20um. dTom: dTomato; DV: Dorsal-Ventral; GFP: Green fluorescent protein; Hh: Hedgehog; mut: mutated; nm: nanometer; UAS: Upstream Activation Sequence; Wt: Wildtype.